International Journal of Heat and Fluid Flow 101 (2023) 109117

Contents lists available at ScienceDirect

International Journal of Heat and Fluid Flow

journal homepage: www.elsevier.com/locate/ijhff

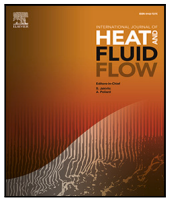

A new perspective on skin-friction contributions in adverse-pressure-gradient turbulent boundary layers

Marco Atzori [a,*], Fermín Mallor [b], Ramón Pozuelo [b], Koji Fukagata [c], Ricardo Vinuesa [b], Philipp Schlatter [b,**]

[a] Department of Particulate Flow Modelling, Johannes Kepler University, Linz, 4040, Austria
[b] SimEx/FLOW, Engineering Mechanics, KTH Royal Institute of Technology, Stockholm, 10044, Sweden
[c] Department of Mechanical Engineering, Keio University, Yokohama, 223-8522, Japan

ARTICLE INFO

Keywords:
Turbulent boundary layers
Adverse pressure gradients
Skin friction

ABSTRACT

For adverse-pressure-gradient turbulent boundary layers, the study of integral skin-friction contributions still poses significant challenges. Beyond questions related to the integration boundaries and the derivation procedure, which have been thoroughly investigated in the literature, an important issue is how different terms should be aggregated. The nature of these flows, which exhibit significant in-homogeneity in the streamwise direction, usually results in cancellation between several contributions with high absolute values. We propose a formulation of the identity derived by Fukagata et al. (2002), which we obtained from the convective form of the governing equations. A new skin-friction contribution is defined, considering wall-tangential convection and pressure gradient together. This contribution is related to the evolution of the dynamic pressure in the mean flow. The results of the decomposition are examined for a broad range of pressure-gradient conditions and different flow-control strategies. We found that the new formulation of the identity allows to readily identify the different regimes of near-equilibrium conditions and approaching separation. It also provides a more effective description of control effects. A similar aggregation between convection and pressure-gradient terms is also possible for any other decomposition where in-homogeneity contributions are considered explicitly.

1. Introduction

The connection between properties of turbulent flows and generation of skin friction is a crucial topic in fluid mechanics with a significant impact on industrial and every-day-life applications. One possible approach to investigate this connection is to derive identities that express the local skin friction in terms of averaged quantities integrated on wall-normal profiles. From a historical point of view, this is the same approach of the von Kármán momentum integral, which is derived in the context of the boundary-layer approximation and that links skin friction and development of the boundary-layer thickness.

In 2002, Fukagata et al. (2002) derived the local skin-friction coefficient as a sum of contributions identified as integral of the non-vanishing terms in the Reynolds-averaged Navier–Stokes equation. This expression, now known as Fukagata–Iwamoto–Kasagi (FIK) identity, has been used in the context of control in both internal flows and boundary layers (Peet and Sagaut, 2009; Mehdi and White, 2011; Kametani and Fukagata, 2011; Kametani et al., 2015; Stroh et al., 2015) and to investigate phenomena such the secondary flow of Prandtl's second kind (Modesti et al., 2018). At the same time, other expressions have been derived using similar procedures with the aim of providing a different perspective or more clear physical interpretation for the contributions. This included relatively natural extension of the derivation *e.g.* incorporating the effects of wall curvature (Monte et al., 2011), or using the conservation of vorticity instead of momentum (Yoon et al., 2016). In the case of turbulent boundary layers (TBLs), the impact of the choice of the upper bound of integration has also been investigated in the past (Mehdi et al., 2014).

In 2016, Renard and Deck (2016) proposed a new identity, denoted as RD decomposition, based on the budget of the turbulent kinetic energy, which improved on the FIK original formulation under two points of view. Firstly, the integrand of the skin-friction contributions have more intuitive scaling properties in the near-wall region and, secondly, in the case of zero-pressure-gradient (ZPG) boundary layers, the integration procedure does not require to establish an upper bound. This is due to adopting a frame of reference where the wall is moving at the free-stream velocity, so that all integrands naturally vanish in

* Corresponding author.
** Second corresponding author.
E-mail addresses: marco.atzori@jku.at (M. Atzori), pschlatt@mech.kth.se (P. Schlatter).

https://doi.org/10.1016/j.ijheatfluidflow.2023.109117
Received 1 November 2022; Received in revised form 27 January 2023; Accepted 10 February 2023
Available online 28 February 2023

the far field. The RD decomposition has been recently used to study internal flows and TBLs, including cases with pressure gradients (Wei, 2018; Fan et al., 2020c,a), compressible flows (Li et al., 2019), and control (Fan et al., 2022). The issue of considering an upper bound of integration, however, still remains in the case with adverse pressure gradients (APGs), because the choice of a reference free-stream velocity is not obvious (the aforementioned studies in these condition still rely on a specific method to identify the boundary-layer edge Fan et al., 2020a, 2022).

How to apply skin-friction decompositions in TBLs in the most effective and meaningful way is still an open question. Recently, Wenzel et al. (2022) employed the FIK decomposition to study compressible TBLs subjected to APG, using a reduced number of integrations, which makes more straightforward the physical interpretation of contributions, and carefully considering the impact of upper bounds. They also applied the same procedure to define contributions for the specific heat-transfer coefficient. On the other hand, Ricco and Skote (2022), demonstrated that the FIK identity is equivalent to the von Kármán integral equation in the limit of infinite upper bounds of integration, and discussed how a finite limit of integration directly affect the decomposition to underline the fundamental challenges of applying it to TBLs.

The aim of the present work is to discuss how cancellations between skin-friction contributions affect the result of the FIK decomposition in APG TBLs. In particular, we focus on the standard FIK identity derived from the averaged momentum conservation in conservative form and on a formulation proposed for boundary layers. In this boundary-layer formulation, (i) the identity is derived from the momentum conservation in convective form, (ii) wall-tangential mean velocity and pressure gradient are considered together, and (iii) the wall-normal convection of vorticity is expressed explicitly. Note that similar cancellations has been already proposed (Atzori et al., 2021a; Wenzel et al., 2022), but without a systematic comparison of the contributions in different forms and examining substantially different pressure-gradient conditions. We consider a vast data set of TBLs subjected to APGs, including both cases developing over a flat plate and the suction side of a NACA4412 airfoil at different Reynolds numbers and angles of attack, and we show how different flow regimes can be identified using the skin-friction contributions. We also consider cases with control, where the high values of contributions in the standard FIK and RD formulation makes it difficult to identify the most relevant control effect (Atzori et al., 2021b).

The paper is organized as follows: in Section 2, we describe the data set and numerical methods; in Section 3, we present the two FIK formulations that we consider; in Section 4, we examine pressure-gradient and control effects on the contributions, and in Section 5, we discuss our conclusions.

2. Data set and numerical methods

We consider several data sets including high-fidelity numerical simulations of incompressible turbulent boundary layers developing both over a flat plate and around a NACA4412 airfoil (see Fig. 1).

For the sake of simplicity, we use a common notation for both flat-plate and airfoil data, where x and y denote the wall-tangential and wall-normal directions, respectively, and U and V are the corresponding mean-velocity components. The airfoil simulations are carried out internally using a global Cartesian frame of reference. The proper tensor rotation is employed for mean velocity components, fluctuations, and derivatives to express each quantity in a local Cartesian frame of reference for any considered wall-normal profile. In the local frame the first and second orthogonal directions are wall-tangential and wall-normal, respectively. Velocity fluctuations with respect to the mean are denoted with u and v so that *e.g.* the Reynolds-shear stress is $\overline{uv}$. The mean pressure is denoted by P. The skin-friction coefficient is defined as $c_f = 2\tau_w/(\rho U_e^2)$, where the wall-shear stress is $\tau_w = \rho\nu(\mathrm{d}U/\mathrm{d}y)_{y=0}$, ρ is the fluid density, and ν is the kinematic viscosity. The subscript e indicates variables at the location of the edge of the boundary layer, denoted by δ_{99}, so that *e.g.* $U_e = U(y = \delta_{99})$. The location of the edge is identified using the method proposed by Vinuesa et al. (2016), based on of the diagnostic scaling (Alfredsson et al., 2011; Drózdz et al., 2015). The length scale used for viscous units is $l^* = \nu/u_\tau$, where the friction velocity is $u_\tau = \sqrt{\tau_w/\rho}$. With this notation, the friction Reynolds number is denoted by $Re_\tau = \delta_{99}u_\tau/\nu$. The Reynolds numbers based on the momentum and displacement thickness are denoted by $Re_\theta = \theta U_e/\nu$ and $Re_\delta = \delta^* U_e/\nu$, respectively, where $\theta = \int_0^{\delta_{99}} U/U_e(1 - U/U_e)\mathrm{d}y$, and $\delta^* = \int_0^{\delta_{99}}(1 - U/U_e)\mathrm{d}y$. We use the Clauser pressure-gradient parameter (Clauser, 1956), denoted by $\beta = \delta^*/\tau_w \mathrm{d}P/\mathrm{d}x|_e$, to provide a qualitative measure of the local pressure-gradient intensity.

The flat-plate data set consists of a zero-pressure-gradient case up to $Re_\theta = 7600$, which we denote ZPG, and five cases with different pressure-gradient conditions. These cases are denoted A1.1, A1.6, A1.6L, A2.8, and A4.5, where the two-digit number refers to the maximum value of β. Note that A.16L differs from A1.6 in the longer domain size and thus range of Reynolds number. The NACA4412 data set includes simulations at angle of attack AoA = 5° at Reynolds numbers based on the chord length $Re_c = 200{,}000$ and 400,000, and at $Re_c = 400{,}000$ with AoA = 11°, which are denoted W5(200k), W5, and W11, respectively. Note that $Re_c = U_\infty c/\nu$, where U_∞ is the velocity of the incoming flow, and c is the chord length. The range of β and Reynolds numbers for the cases mentioned so far are reported in Table 1.

The NACA4412 data set also includes three cases with control applied on the suction side in region $0.25 < x/c < 0.86$, with uniform blowing, uniform suction, and body-force damping. The body-force case is a model for the effects of opposition control (Stroh et al., 2016). These control cases are denoted by W5BL, W5SC, and W5BF, respectively. In the two cases W5BL and W5SC, the control intensity is $0.1\%U_\infty$, while the case with body-force damping is designed so that the control have effects similar to that in W5BL. Hereafter, we provide a brief summary of the numerical methods that have been employed and of the overall flow properties in each case.

2.1. Flat plate

The flat-plate TBL simulations are well-resolved large-eddy simulations (LESs) performed with the pseudo-spectral code *SIMSON* (Chevalier et al., 2007) and using the approximate deconvolution relaxation-term (ADM-RT) sub-grid model (Schlatter et al., 2004). The ZPG case (Eitel-Amor et al., 2014) was validated with direct-numerical-simulation (DNS) data (Schlatter and Örlü, 2010). The APG cases used a similar numerical setup (Bobke et al., 2016, 2017; Pozuelo et al., 2022), and case A1.6L was compared and validated against experimental data (Vila et al., 2020). In these simulations, the resolution in space in the three direction is approximately $(\Delta x^+, \Delta y^+, \Delta z^+) < (20, 0.2 - 30, 10)$, where the highest Δy^+ is referred to the region above the boundary-layer edge at high Reynolds number. Only a portion of the original data set is considered in the present study due to the different statistical convergence at different streamwise locations. The skin-friction coefficient and Clauser parameter for these cases are shown in Fig. 2 as functions of Re_θ. This data set was created to study the influence of history effects on the local properties of the boundary layer, *i.e.* how inner-scaled profiles of velocity and turbulent fluctuations can differ even at matching values of β and Re_τ. In A1.1, A1.6, A2.8, and A4.5, β increases with a similar rate up to the different maximum values, while in A1.6L the evolution of β is slower, resulting in a different streamwise evolution of c_f in each case.

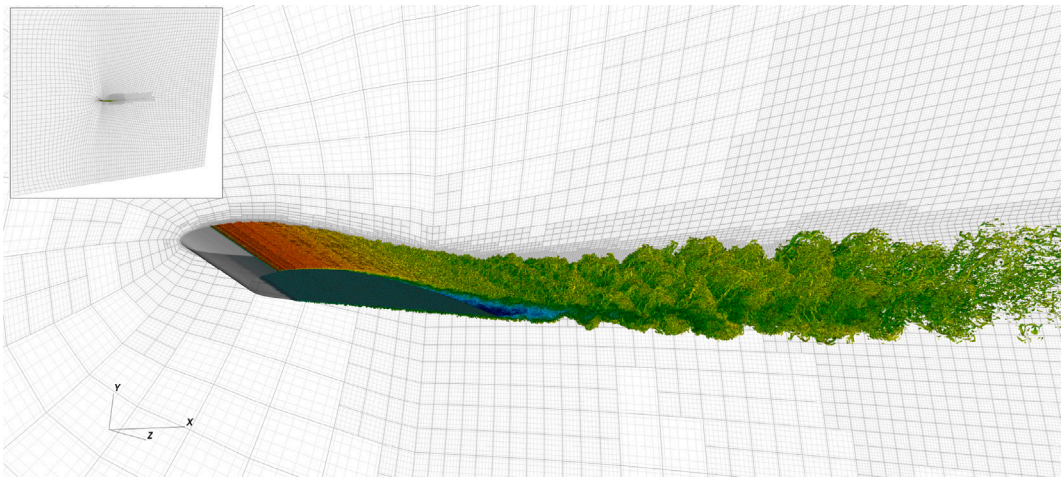

Fig. 1. Overview of the NACA4412 simulation at angle-of-attack 11 and Re_c = 400,000, showing instantaneous vortex clusters. The structures are identified with the λ_2 criterion (Jeong and Hussain, 1995) and colored with the streamwise velocity (where dark blue denotes −0.5 and dark red 2.5). The simulation is performed with *Nek5000* (Fischer et al., 2008), using adaptive mesh refinement (Tanarro et al., 2020). The entire computational domain is shown in the insert. (For interpretation of the references to color in this figure legend, the reader is referred to the web version of this article.)

Table 1
Range of the pressure gradient parameter (β) and Reynolds numbers based on the friction velocity, the momentum thickness, and the displacement thickness (Re_τ, Re_θ, and Re_δ, respectively) for the considered cases without control. Note that for the airfoils (three last columns on the left), the values refer to the region $0.4 < x/c < 0.8$.

β	ZPG ≈0	A1.1 0–4.5	A1.6 0–2.8	A1.6L 0–1.6	A2.8 0–1.6	A4.5 0–1.1	W5(200k) 0.6–5.8	W5 0.6–4.9	W11 1.3–48
Re_τ	160–2300	150–700	160–740	180–1600	160–770	160–750	160–225	240–360	260–380
Re_θ	340–7600	320–4000	330–3600	380–7400	330–3200	320–3100	450–1100	760–1800	1100–3000
Re_δ	550–10 400	530–7400	530–6200	600–11 400	530–5000	520–4800	770–2100	1200–3300	1700–7700

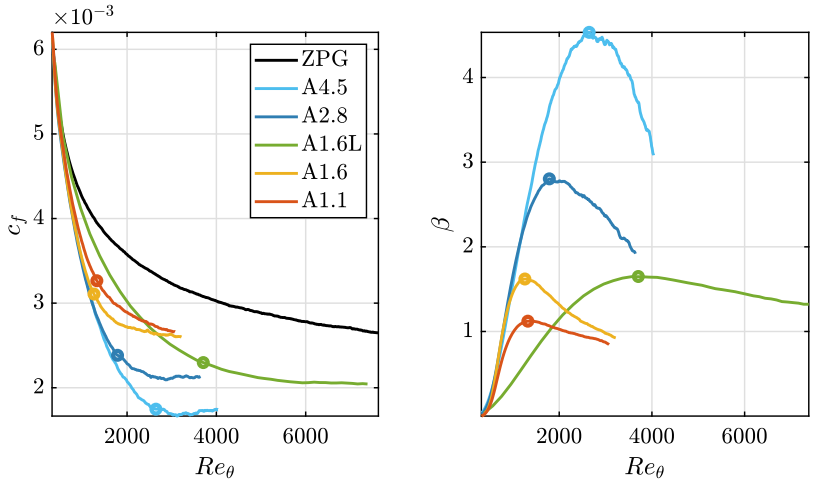

Fig. 2. (Left) Skin-friction coefficient, denoted by c_f and (right) Clauser pressure-gradient parameter, denote by β, for the flat-plate cases. The circles denote the location of maximum β.

2.2. Airfoil

The wing simulations considered in this work are well-resolved LES carried out with the code *Nek5000* (Fischer et al., 2008), which is based on the spectral-element method (Patera, 1984) (SEM). The LES filter is based again on the same ADM-RT sub-grid model (Schlatter et al., 2004) as for the flat-plate simulations, which was validated for this setup with DNS data (Hosseini et al., 2016) for the reference case at Re_c = 400,000, showing excellent agreement in mean profiles, velocity fluctuations and terms of the turbulent-kinetic-energy budget (Vinuesa et al., 2018; Negi et al., 2018), in addition to instantaneous flow structures (Eitel-Amor et al., 2014). The cases at AoA = 5° have been simulated using a conformal C-type mesh that extends up to a distance of $2c$ in each direction from the airfoil surface, and at least $0.1c$ in the spanwise direction (Vinuesa et al., 2018; Atzori et al., 2021b). A RANS simulation provides boundary conditions at the inlet and upper and lower sides, and a local-stress outflow condition is used for the rear side of the domain (Dong et al., 2014). The mesh is designed using the wall-shear stress of RANS simulations so that the resolution in the turbulent region of the domain is approximately $(\Delta x^+, \Delta y^+, \Delta z^+) < (18, 0.64 - 11, 9)$. Note that the case with body-force damping is examined here for the first time, but it is analogous to a previous one with the same control at Re_c = 200,000 (Atzori et al., 2021b). The case at AoA = 11° is also examined here for the first time and uses a different setup, taking advantage of the recent implementation of adaptive mesh refinement in *Nek5000* (Tanarro et al., 2020). In particular, the grid

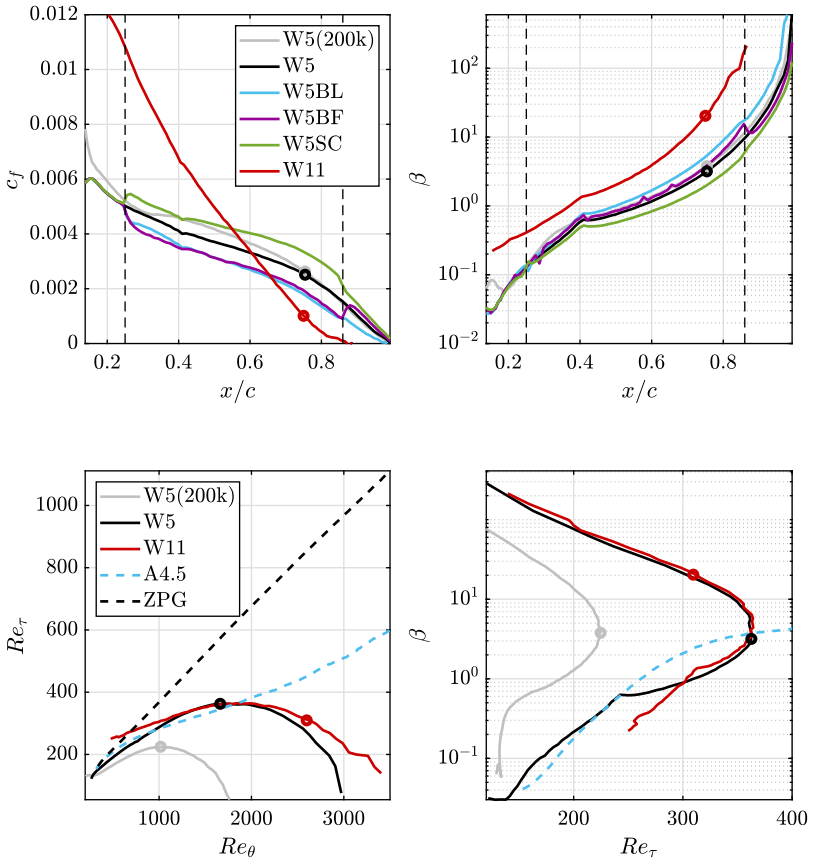

Fig. 3. (Top, left and right) Skin-friction coefficient and Clauser pressure-gradient parameter for the suction side of the NACA4412 cases, respectively. The dashed vertical lines denote the control region. (Bottom, left and right) Friction Reynolds number as a function of Re_θ, and Clauser parameter as a function of Re_τ, respectively. The circles in each plot denote location $x/c = 0.75$.

for the production case is obtained by progressively refining an initial mesh with *h-type* refinement, *i.e.* dividing spectral elements where it is needed, which is determined using a spectral error indicator (Mavriplis, 1990). The resulting mesh is non-conformal with a resolution in the turbulent region similar to that of the previous cases, allowing to use a much larger domain size that extents for $50c$, $40c$ and $0.6c$ in the horizontal, vertical and spanwise directions, respectively. The larger size of the domain reduces the impact of the boundary conditions and allows to properly describe the large turbulent structures in separation conditions. In all wing simulations, transition to turbulence is induced at a distance from the leading edge of $x/c = 0.1$ using a random volume force with given intensity and length and time scales, implemented to simulate tripping devices in experiments (Schlatter and Örlü, 2012).

To provide an overview of these data sets, we show the skin friction and Clauser parameters as functions of the distance from the leading edge for all wing cases in Fig. 3, together with Re_θ as a function of Re_τ and β as a function of Re_τ for the cases without control and the flat-plate cases ZPG and A4.5. The local skin-friction decreases for all cases due to the progressively stronger APG. Uniform blowing and suction have approximately opposite effects, decreasing and increasing c_f, respectively. The amplitude of the body-force damping is calibrated to produce a similar skin-friction reduction in the case with uniform blowing in the control region, but c_f rapidly recovers further downstream (as previously observed on flat plate Stroh et al., 2016). The development of β is very similar for the two cases W5(200k) and W5, which only differ for the value of Re_c. The streamwise evolution Re_τ in the wing cases is significantly affected by the pressure gradient. In internal-flow canonical cases, such as turbulent channel or pipe, and in ZPG TBLs, Re_τ is an indicator of the separation that exists between the smallest and the largest scales that are present in the turbulent boundary layer and thus increases monotonically if the macroscopic Reynolds number increases. This still holds true for the APG flat-plate cases, even though Re_τ is reduced compared with the corresponding ZPG TBL. For the cases examined in the wing however, Re_τ is still increasing only up to a certain streamwise location, after which u_τ decreases faster than the growth of δ_{99}, causing Re_τ to also decrease.

3. FIK identity for boundary layers

The FIK identity is derived applying a triple integration by parts to the (partially) averaged Navier–Stokes equation (Fukagata et al., 2002). This procedure results in a collection of terms, depending on the symmetry of the considered case. In the case of simulations of turbulent channel, where periodic boundary conditions are imposed in both the streamwise and spanwise directions, the total c_f is expressed as:

$$c_f = \frac{12}{Re_b} + 12 \int_0^2 (1-y)(-\overline{uv})\,\mathrm{d}y\,, \tag{1}$$

where $Re_b = U_b H/\nu$ is the Reynolds number computed with bulk velocity U_b and the full channel height H. In the case of turbulent boundary layers however, the flow is non-homogeneous in the streamwise direction and terms including derivatives in that direction do not vanish. Other identities, although derived with a different methodology, also result in similar collections of terms. In the present section, we summarize the terms of the FIK decomposition obtained from the conservative form of the averaged Navier–Stokes equations, which we referred to as "standard" formulation, and we consider a "boundary-layer" formulation.

3.1. Standard formulation

The standard formulation of the FIK identity is derived applying a triple integration by parts to the averaged streamwise momentum

conservation, which reads:

$$\frac{\partial(U^2)}{\partial x}+\frac{\partial(UV)}{\partial y}=-\frac{\partial P}{\partial x}+\nu\left(\frac{\partial^2 U}{\partial y^2}+\frac{\partial^2 U}{\partial x^2}\right)-\frac{\partial\overline{uv}}{\partial y}-\frac{\partial\overline{u^2}}{\partial x}\,. \tag{2}$$

This procedure results in the following identity:

$$c_f=c_f^{\delta}+c_f^{T}+c_f^{D}+c_f^{P}\,, \tag{3}$$

where each contribution is defined as:

$$c_f^{\delta}=4\frac{1-\delta^*/\delta_{99}}{Re_\delta}\,, \tag{4}$$

$$c_f^{T}=-4\int_0^1(1-\eta)\overline{uv}\,\mathrm{d}\eta\,, \tag{5}$$

$$c_f^{D}=-2\int_0^1(1-\eta)^2 I_x\,\mathrm{d}\eta\,, \tag{6}$$

$$c_f^{P}=-2\int_0^1(1-\eta)^2\frac{\partial P}{\partial x}\,\mathrm{d}\eta\,. \tag{7}$$

The first contribution directly takes into account the evolution of the boundary-layer thickness. The second contribution takes into account turbulent fluctuations. The third contribution includes all terms which would vanish in case of flows homogeneous in the streamwise direction, and the four contributions includes explicitly the pressure gradients. The multiplicative factors $(1-\eta)^n$ are a result of the integration by parts, and $\eta=y/\delta_{99}$ is the outer-scaled wall-normal location. When the FIK contributions are derived from the conservative form of the governing equations, the term I_x is written as:

$$I_x=\frac{\partial(U^2)}{\partial x}+\frac{\partial(\overline{u^2})}{\partial x}+\frac{\partial(UV)}{\partial y}-\frac{1}{Re_\delta}\frac{\partial^2 U}{\partial x^2}\,. \tag{8}$$

Contributions c_f^D can thus be expressed as the sum of four additional terms, as follows:

$$c_f^{D1}=-2\int_0^1(1-\eta)^2\frac{\partial(UU)}{\partial x}\,\mathrm{d}\eta, \tag{9}$$

$$c_f^{D2}=-2\int_0^1(1-\eta)^2\frac{\partial\overline{u^2}}{\partial x}\,\mathrm{d}\eta, \tag{10}$$

$$c_f^{D3}=-2\int_0^1(1-\eta)^2\frac{\partial(UV)}{\partial\eta}\,\mathrm{d}\eta, \tag{11}$$

$$c_f^{D4}=-2\int_0^1(1-\eta)^2\left(-\frac{1}{Re_\delta}\frac{\partial^2 U}{\partial x^2}\right)\mathrm{d}\eta. \tag{12}$$

Of these four contributions, c_f^{D1} and c_f^{D3}, which are directly related with mean-velocity components, tend to be the most relevant of the non-homogeneous contributions.

3.2. Boundary-layer formulation

For the case of turbulent boundary layers, we propose a new formulation following three steps. The first step is simply to combine c_f^{D1} and c_f^{D3} using the continuity equation, which is equivalent to deriving the FIK identity from the convective form of the governing equations. In this case, the integrand of the non-homogeneous contribution, c_f^D, reads:

$$I_x^*=U\frac{\partial U}{\partial x}+\frac{\partial(\overline{u^2})}{\partial x}+V\frac{\partial U}{\partial y}-\frac{1}{Re_\delta}\frac{\partial^2 U}{\partial x^2}\,, \tag{13}$$

resulting in different contributions from mean convection instead of c_f^{D1} and c_f^{D3}. We denote the corresponding new contributions c_f^{D1*} and c_f^{D3*}, respectively:

$$c_f^{D1*}=-2\int_0^1(1-\eta)^2 U\frac{\partial U}{\partial x}\,\mathrm{d}\eta, \tag{14}$$

$$c_f^{D3*}=-2\int_0^1(1-\eta)^2 V\frac{\partial U}{\partial\eta}\,\mathrm{d}\eta. \tag{15}$$

The second step is to introduce a contribution which contains the mean spanwise vorticity, denoted by $\Omega_z=\partial V/\partial x-\partial U/\partial y$. The new contribution related to wall-normal convection, c_f^{D3*}, is thus substituted by two new terms in the boundary-layer formulation:

$$c_f^{D\Omega}=+2\int_0^1(1-\eta)^2 V\Omega_z\,\mathrm{d}\eta\,, \tag{16}$$

$$c_f^{DV}=-2\int_0^1(1-\eta)^2\left(V\frac{\partial V}{\partial x}\right)\mathrm{d}\eta\,. \tag{17}$$

The third step is to consider together the streamwise-convection term, c_f^{D1*}, the new c_f^{DV} term, and the pressure-gradient term, creating the following contribution:

$$c_f^{DP}=-2\int_0^1(1-\eta)^2\left(U\frac{\partial U}{\partial x}+V\frac{\partial V}{\partial x}+\frac{\partial P}{\partial x}\right)\mathrm{d}\eta\,. \tag{18}$$

This step is motivated with the following reasoning. For points along streamlines in the inviscid flows, we can write the Bernoulli equation as:

$$\frac{1}{2}\rho(U^2+V^2)+P=P_0\,, \tag{19}$$

where P_0 denotes the total pressure, which is constant along streamlines, and $q=1/2[\rho(U^2+V^2)]$ is the dynamic pressure. The derivatives of this expression in the wall-tangential direction in the inviscid flow is then:

$$U\frac{\partial U}{\partial x}+V\frac{\partial V}{\partial x}+\frac{\partial P}{\partial x}=0\,. \tag{20}$$

The new contribution c_f^{DP} is thus defined with the spirit of removing the apparent contributions to friction that are related to the development of the irrotational flow above the boundary layer and to acknowledge the fact that mean convection and pressure gradient remain partially connected even in the turbulent boundary layer. We name this new term "dynamic-pressure contribution" hereafter, as it describes the balance between the evolution of the dynamic pressure in the mean flow and the pressure gradient.

The relation between the boundary-layer and standard FIK formulations can be summarized by the following identities between the contributions related to mean convection and pressure gradient:

$$c_f^{DP}-c_f^{DV}=c_f^{D1*}+c_f^{P}=\frac{1}{2}c_f^{D1}+c_f^{P}\,, \tag{21}$$

$$c_f^{D\Omega}+c_f^{DV}=c_f^{D3*}=\frac{1}{2}c_f^{D1}+c_f^{D3}\,. \tag{22}$$

The sum of these expressions yields $c_f^{DP}+c_f^{D\Omega}=c_f^{D1}+c_f^{D3}+c_f^{P}$, which is a direct consequence of the fact that the standard and boundary-layer formulations are equivalent. The definitions of all contributions in both formulations are reported in Table 2.

Note that Wenzel et al. (2022) used a similar approach for the study of compressible TBLs to have better cancellations between the contributions of FIK identity derived from a double integration by parts. In their case, wall-tangential convection and pressure gradient are considered together, but the different form of the Bernoulli equation for compressible flows makes the interpretation of the resulting spatial-development term less intuitive.

The definition of the upper bound of integration has been considered a critical point in the application of the FIK decomposition and

Table 2
Definition of skin-friction contributions in both FIK formulations.

Standard formulation	Boundary-layer formulation
$c_f^{D1}=-2\int_0^1(1-\eta)^2\frac{\partial(UU)}{\partial x}\,\mathrm{d}\eta$ $c_f^{D3}=-2\int_0^1(1-\eta)^2\frac{\partial(UV)}{\partial\eta}\,\mathrm{d}\eta$	$c_f^{DP}=-2\int_0^1(1-\eta)^2\frac{\partial}{\partial x}\left(\frac{1}{2}(U^2+V^2)+P\right)\mathrm{d}\eta$
$c_f^{P}=-2\int_0^1(1-\eta)^2\frac{\partial P}{\partial x}\,\mathrm{d}\eta$	$c_f^{D\Omega}=+2\int_0^1(1-\eta)^2 V\Omega_z\,\mathrm{d}\eta$
$c_f^{\delta}=4\frac{1-\delta^*/\delta_{99}}{Re_\delta}$	$c_f^{\delta}=4\frac{1-\delta^*/\delta_{99}}{Re_\delta}$
$c_f^{T}=4\int_0^1(1-\eta)\overline{uv}\mathrm{d}\eta$	$c_f^{T}=4\int_0^1(1-\eta)\overline{uv}\mathrm{d}\eta$
$c_f^{D2}=-2\int_0^1(1-\eta)^2\frac{\partial\overline{u^2}}{\partial x}\,\mathrm{d}\eta$	$c_f^{D2}=-2\int_0^1(1-\eta)^2\frac{\partial\overline{u^2}}{\partial x}\,\mathrm{d}\eta$
$c_f^{D4}=-2\int_0^1(1-\eta)^2\left(-\frac{1}{Re_\delta}\frac{\partial^2 U}{\partial x^2}\right)\mathrm{d}\eta$	$c_f^{D4}=-2\int_0^1(1-\eta)^2\left(-\frac{1}{Re_\delta}\frac{\partial^2 U}{\partial x^2}\right)\mathrm{d}\eta$

similar identities in the general context of the TBL (*e.g.* by Ricco and Skote (2022)). These analyses have been focused on the ZPG case, where the zero wall-normal gradient of U in the irrotational region allows extending the integration bound in the limit of $y \to \infty$. However, in case of pressure gradients or other modifications of the free-stream flow, the choice of a local reference U_∞ is equivalent to a choice of the upper limit of the boundary layer. We assume that a definition of the boundary-layer thickness is provided and that it is consistent with the flow development. The results shown hereafter are obtained using δ_{99} based on the diagnostic scaling, as mentioned in Section 2. Previous studies reported only a small dependency of the contributions for small changes of δ_{99}, as expected from the shape of the integration pre-factor and the properties of the flow (Atzori et al., 2021b). It is also worth mentioning that Griffin et al. (2021) recently proposed a method to identify δ_{99} based on a comparison between the mean velocity in the TBL and the expected velocity from the irrotational free-stream flow. This method uses a condition naturally similar to the definition of c_f^{DP} and it yields values of δ_{99} in very good agreement to the one used in the present paper, if a consistent condition for the edge location is used. In this context, we can then state that the FIK identity is used in the present form to study the balance of contributions in the domain region within the turbulent boundary layer. A different definition of the integration bound, *e.g.* with a value of $1.5\delta_{99}$ or higher, will naturally lead to different results, as a larger portion of irrotational flow is included. We will examine the sensitivity of contributions with respect to the choice of the upper integration bound in Section 4.2.

We also note that the same aggregation for terms related to streamwise development of the mean flow and pressure gradients can be proposed for decompositions that are derived in a similar way from the governing equations. This is for instance the case of *e.g.* the RD decomposition, if the non-homogeneous contribution is expressed in explicit form (see Appendix A). In the case of the angular-momentum integral (AMI) equation proposed by Elnahhas and Johnson (2022), the same approach could also be applied at least from a formal point of view. It does not seem entirely appropriate however because the contributions are already defined in terms of the defect profiles from the von Kármán momentum integral to distinguish between laminar and turbulent contributions (see Appendix B).

4. Results

In this section, we examine the FIK contributions for a selected set of pressure-gradient conditions. We focus on how the boundary-layer formulation can improve the description of both pressure-gradient and control effects, and on how the new dynamic-pressure contribution can be used to identify different flow regimes.

4.1. APG effects over the flat plate

Firstly, we compare the canonical zero-pressure-gradient TBL and the adverse-pressure-gradient TBL in case A1.6L, which exhibits moderate values of β. Fig. 4 shows the skin-friction contributions and the relative skin-friction contributions in both cases and for both formulations as functions of Re_θ. The values of the relative contributions for three selected locations are reported in Table 3. The relative contributions are normalized with the total c_f of each case, so that their sum is 1. Note that the qualitative development of relative contributions may differ from that of absolute contributions, depending on the rate of the change of c_f. For example, a relative contribution will still increase even when the corresponding absolute contribution decreases, if c_f decreases faster.

When compared against the ZPG case, APG TBLs exhibit a faster decrease of c_f as the boundary-layer develops, which is also matched by a qualitative change in the FIK contributions. The turbulent-fluctuation contribution, c_f^T, which has the same expression in both FIK formulations, progressively decreases in the ZPG case but it increases in the streamwise region that approximately coincides with the increase of β.

Table 3
Relative skin-friction contributions of the FIK identity in the ZPG and A1.6L cases at selected locations. Contributions that appear in the standard and boundary-layer formulations are denoted with (S) and (BL), respectively. The sum is reported in the last line (the value of 1.01 for the last case is caused by statistical uncertainty).

	ZPG			A1.6L		
β	0	0	0	1.2	1.6	1.4
Re_θ	2000	4000	6000	2000	4000	6000
Re_τ	680	1300	1800	530	850	1200
c_f^T/c_f (S & BL)	**0.74**	**0.77**	**0.78**	1.20	1.62	1.68
$(c_f^\delta + c_f^{D2} + c_f^{D4})/c_f$ (S & BL)	0.06	0.02	0.02	0.09	0.08	0.05
c_f^{D1}/c_f (S)	0.48	0.48	0.45	**3.54**	**3.87**	**3.20**
c_f^{D3}/c_f (S)	−0.28	−0.27	−0.25	−2.14	−2.35	−1.90
c_f^P/c_f (S)	0	0	0	−1.69	−2.22	−2.02
c_f^{DP}/c_f (BL)	0.24	0.24	0.22	0.08	−0.28	−0.42
$c_f^{D\Omega}/c_f$ (BL)	−0.04	−0.03	−0.02	−0.37	−0.42	−0.30
$\sum_X c_f^X/c_f$	1.00	1.00	1.00	1.00	1.00	1.01

Already for the ZPG case, the contributions are significantly different between the standard and boundary-layer formulations. In particular, in the standard formulation, both c_f^{D1} and c_f^{D3} have not-negligible values, albeit lower than c_f^T. In the boundary-layer formulation however, $c_f^{D\Omega}$ only reaches low values, *e.g.* −3% of c_f at $Re_\theta = 4000$ instead of −27% of the corresponding c_f^{D3}. This immediately clarifies that wall-normal convection is actually negligible in the ZPG case. The boundary-layer formulation then shows that skin friction is generated in ZPG TBL mainly as a combination of the turbulent fluctuations and the dynamic-pressure contributions.

The three contributions c_f^{D1}, c_f^{D3}, and c_f^P are the more relevant ones for the standard FIK formulation in the APG case. The streamwise-convection contribution, c_f^{D1}, is positive, while the wall-normal convection and pressure gradient contributions, c_f^{D3} and c_f^P, respectively, are negative. All these terms have absolute values that are relatively high. In particular, c_f^{D1} reaches up to 4 times the total c_f in case A1.6L. These contributions are also higher than c_f^T for the APG case at every Re_θ and β. The streamwise development of the standard FIK contributions also suggests that a change of regime is occurring at a certain Re_θ slightly above 2000, where the absolute values of c_f^{D1}, c_f^{D3}, and c_f^P start to decrease. However, it is not immediately possible to identify whether this change of regime modifies the balance among the various terms. In the boundary-layer formulation, on the other hand, c_f^{DP} and $c_f^{D\Omega}$ are lower than c_f^T and the sign of c_f^{DP} immediately describes the balance between streamwise convection and pressure gradient. In case A1.6L, this term is initially positive but it decreases and changes sign at $Re_\theta \approx 2500$. At the same time, $c_f^{D\Omega}$ is always negative, it initially decreases up to $Re_\theta \approx 2500$, and then it increases farther downstream.

Of the remaining terms, the most relevant is c_f^δ, but this contribution is always decreasing for both ZPG and APG cases as the Reynolds number increases. On the other hand, c_f^{D4} is slightly increasing but still remains very low. Overall, these terms are all progressively less relevant at higher Reynolds number, so that the sum of the larger ones accounts for *e.g.* 98% and 96% of c_f at $Re_\theta = 6000$ for ZPG and A1.6L, respectively. This result is the same for both formulations, due to the extremely low values of c_f^{DV}.

We now focus on the region of rapidly increasing β before $Re_\theta \approx 3000$ to discuss more in detail the behavior of the new contributions c_f^{DP} and $c_f^{D\Omega}$, also considering the other flat-plate cases. Compared to A1.6L, these cases exhibit a higher rate of change of β in the aforementioned region. For instance, case A1.6 reaches $\beta = 1.6$ at $Re_\theta = 1260$ while case A1.6L reaches the same value at $Re_\theta = 3700$. The faster increase of β results in more pronounced APG effects, as TBLs tend to be less sensitive to pressure gradient at higher Reynolds numbers. This is firstly illustrated by a higher c_f^T relative contribution, which increases approximately up to the location of maximum β (Fig. 5, left). However, it is

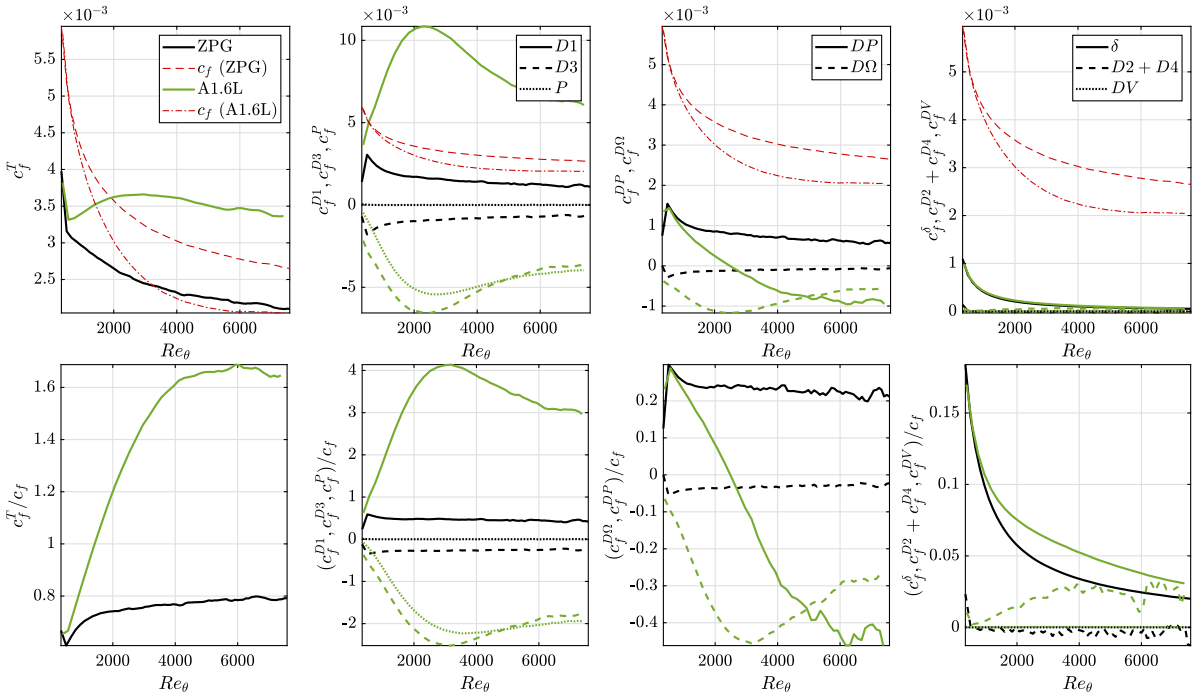

Fig. 4. (Top row) Contributions and (Bottom row) relative contributions to the skin friction for cases ZPG and A1.6L, calculated using both the standard and boundary-layer FIK formulations.

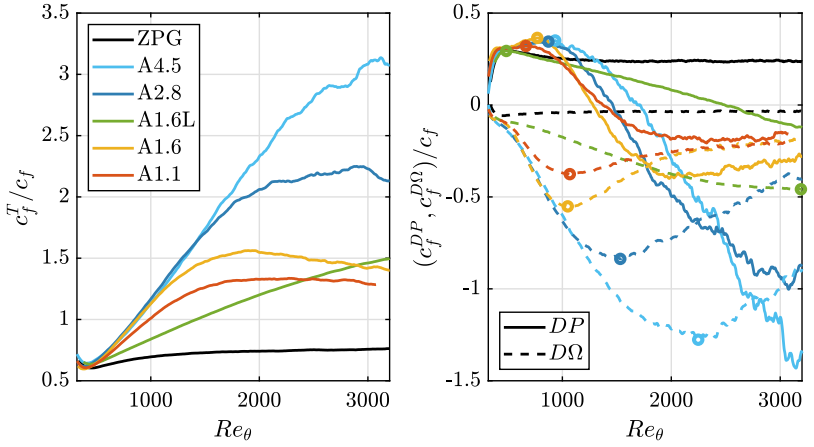

Fig. 5. Relative contributions related to (left) turbulent fluctuations and (right) dynamic pressure and wall-normal convection for all flat-plate cases.

the behavior of c_f^{DP} and $c_f^{D\Omega}$ that exhibits more important differences for different developments of β (Fig. 5, right). The relative contribution of the dynamic pressure c_f^{DP}/c_f increases over a longer streamwise region in the cases with faster growth of β. At the same time, $c_f^{D\Omega}/c_f$ reaches a lower value in these cases than in A1.6L. In all flat-plate cases, c_f^{DP} decreases and eventually changes sign while $c_f^{D\Omega}$ remains negative but increases at higher Re_θ when pressure-gradient effects are less strong. To better describe the streamwise evolution of the dynamic-pressure and vorticity-convection contributions, we report in Table 4 two indicators of the development of β, *i.e.* the location of maximum β and the location of the maximum rate of change of β, together with the position and value of the maximum of c_f^{DP}/c_f and the minimum of $c_f^{D\Omega}/c_f$. The rate of change of β is defined as $\mathrm{d}\beta/\mathrm{d}x$ and it is considered here to give a qualitative indication of the streamwise evolution of β.

It appears that c_f^{DP} is particularly sensitive to the variation of pressure-gradient conditions, as shown by the following observations. On the one hand, for cases A1.1, A1.6, and A2.8, the location of highest $\mathrm{d}\beta/\mathrm{d}x$ is close to that of the maximum of c_f^{DP}. For case A4.5, the maximum of c_f^{DP}/c_f appears upstream than that of $\mathrm{d}\beta/\mathrm{d}x$, and in fact in a location similar to that of case A2.8. For case A1.6L, the location of maximum c_f^{DP} is even more upstream than the location of maximum

Table 4
Locations of maximum β, maximum rate of change of β, maximum c_f^{DP}/c_f and minimum $c_f^{D\Omega}/c_f$, and values of c_f^{DP}/c_f and $c_f^{D\Omega}/c_f$ and the location of their extrema.

	A1.1	A1.6	A2.8	A4.5	A1.6L
$Re_\theta(\max[\beta])$	1300	1300	1800	2600	3700
$Re_\theta(\max[\mathrm{d}\beta/\mathrm{d}x])$	690	710	880	1200	1400
$Re_\theta(\max[c_f^{DP}/c_f])$	670	770	870	930	490
$\max[c_f^{DP}/c_f]$	0.32	0.37	0.35	0.35	0.29
$Re_\theta(\min[c_f^{D\Omega}/c_f])$	1100	1000	1500	2200	3200
$\min[c_f^{D\Omega}/c_f]$	−0.38	−0.55	−0.84	−1.30	−0.46

Table 5
Impact of the definition of the integration upper limit on the relative skin-friction contributions of the boundary-layer FIK formulation. Bold font denotes values obtained if the integration limit is $\delta_e = \delta_{99}$, which are the same as those reported in Table 3 for the same cases and Re_θ. The sum of all relative contributions is denoted by $\sum_X c_f^X/c_f$.

ZPG ($\beta = 0$, $Re_\theta = 4000$, $Re_\tau = 1300$)					
δ_e/δ_{99} (%)	100	101	105	110	125
k_e/k_{99} (%)	100	93	66	42	10
$c_f \times 10^3$	**3.09**	3.08	3.05	3.03	3.00
c_f^T/c_f	**0.77**	0.77	0.76	0.74	0.70
c_f^{DP}/c_f	**0.24**	0.24	0.26	0.28	0.33
$c_f^{D\Omega}/c_f$	**−0.03**	−0.03	−0.04	−0.04	−0.05
$(c_f^\delta + c_f^{D2} + c_f^{D4})/c_f$	**0.02**	0.02	0.02	0.02	0.02
$\sum_X c_f^X/c_f$	1.00	1.00	1.00	1.00	1.00
A1.6L ($\beta = 1.6$, $Re_\theta = 4000$, $Re_\tau = 850$)					
δ_e/δ_{99} (%)	100	101	105	110	125
k_e/k_{99} (%)	100	90	58	33	8
$c_f \times 10^3$	**2.28**	2.28	2.26	2.25	2.25
c_f^T/c_f	**1.62**	1.62	1.59	1.57	1.49
c_f^{DP}/c_f	**−0.28**	−0.27	−0.21	−0.14	0.08
$c_f^{D\Omega}/c_f$	**−0.42**	−0.43	−0.46	−0.51	−0.64
$(c_f^\delta + c_f^{D2} + c_f^{D4})/c_f$	**0.08**	0.08	0.08	0.08	0.07
$\sum_X c_f^X/c_f$	1.00	1.00	1.00	1.00	1.00

$\mathrm{d}\beta/\mathrm{d}x$. In all cases, the change from a regime of increasing c_f^{DP}/c_f to a regime of decreasing c_f^{DP}/c_f is thus not related with location of maximum β, but rather with how fast β is increasing. Decreasing after its maximum, c_f^{DP} eventually becoming negative. The wall-normal convection of vorticity adapts to changes in the pressure conditions more slowly than c_f^{DP}. This contribution is always negative and decreases up a location which is slightly upstream that of the maximum of β, after which increases approaching zero from below.

The results analyzed in this section show that there are different mechanisms that lead to the faster rate at which c_f decreases in APG cases with respect to the ZPG TBL, as illustrated by the balance between various skin-friction contributions. This fact is a direct consequence of the different sensitivity of the contributions to change in pressure conditions, in particular in the case of c_f^{DP} and $c_f^{D\Omega}$.

4.2. Sensitivity related to the integration limit

We now introduce δ_e to denote a generic measure of the boundary-layer thickness that determines the upper limit of integration of the FIK contributions. In the present section we address the impact of a change of δ_e, while in both the previous and in the subsequent sections δ_e is δ_{99}. A key point in this analysis is to establish what the appropriate range of values for δ_e is and we argue that it needs to be consistent with the idea that the analysis is limited to the turbulent region of the domain, *i.e.* the "boundary edge". We thus select five values from δ_{99} to $1.25\delta_{99}$. We focus on two cases examined in the previous section, *i.e.* ZPG and A1.6L, at the locations where $Re_\theta = 4000$, and we limit this analysis to the boundary-layer formulation. Similar results are obtained at different locations for this data set and are thus not shown here. The relative contributions are reported in Table 5, together with the values of δ_e expressed in percentage of δ_{99}. To quantify how the turbulent intensity varies at the integration bound, we also introduce the turbulent kinetic energy at δ_e, denoted by $k_e = k(y = \delta_e)$, where $k = (\overline{u^2} + \overline{v^2} + \overline{w^2})/2$, and the same quantity if $\delta_e = \delta_{99}$, denoted by k_{99}. Finally, it is worth mentioning that a change in the integration bound also corresponds to a change of U_e, which modifies the local scaling (and thus value) for c_f.

The first value of δ_e is 1% higher than δ_{99}, and results in virtually no changes in the contributions; in particular, only c_f^{DP} and $c_f^{D\Omega}$ in case A1.6L are affected, and only by an amount equal to 1% of the total c_f. For the second value of δ_e, which is 5% higher than δ_{99}, the three most relevant contributions are slightly modified in both the zero-pressure-gradient and the adverse-pressure-gradient cases, but this change of δ_e still causes a discrepancy of the order of only few percentage points of c_f. It is important to note that, while variations of the integration bound from $\delta_e = \delta_{99}$ up to $\delta_e = 1.05\delta_{99}$ may appear modest, they cause a quite significant reduction in the turbulent kinetic energy at δ_e. This rapid decrease, which is in fact characteristic of the edge of turbulent boundary layers, has often been documented and also employed to develop tracking criteria for the instantaneous turbulent-non-turbulent interface (TNTI) (Chauhan et al., 2014; Atzori et al., 2020). The two larger values of δ_e, *i.e.* $1.1\delta_e$ and $1.25\delta_e$, finally lead to differences for the c_f^{DP} contribution in case A1.6L of more than $10\%c_f$ and, at $\delta_e = 1.25\delta_e$, c_f^{DP} experiences even a change of sign.

However, the three more relevant contributions of the boundary-layer FIK are not equally affected by the change of integration limit, and are more sensitive in the APG case. To describe how exactly a change in the integration bound produces a modification of the contributions, we examine wall-normal profiles of the integrands. The integrand for a generic contribution c_f^X is denoted by γ_f^X and includes all scaling factors and numerical constants. These quantities are shown premultiplied by y^+ in Fig. 6. We also include in the same figure the inner-scaled mean velocity, wall-tangential fluctuations, and Reynolds-shear stress to give a general description of the state of the TBL. The comparison between the turbulence statistics in the ZPG and A1.6L cases highlights the pressure-gradient effects in the latter. In particular, it is possible to identify the higher inner-scaled wall-tangential velocity in the wake region of the boundary layer and the emergence of a secondary peak in the velocity fluctuations.

The premultiplied profiles of the integrands for the various values of δ_e reflect the different sensitivity of the contributions. It is important to note that the contributions change values not just as a direct consequence of the larger integration domain, but more specifically because of the change of the weight factors $(1-\eta)^n$ due to the integration by parts. If we exclude $\gamma_f^{D\Omega}$ in the ZPG case, for which the corresponding contribution is very small, γ_f^T is the least affected for both ZPG and A1,6L. For this integrand, the progressive increase of δ_e results in a lower portion of the contribution from the region closer to the wall, which explains the progressive reduction of c_f^T. On the other hand, the increase of δ_e corresponds to an increase of γ_f^{DP} and of the absolute value of $\gamma_f^{D\Omega}$ in the region farther from the wall. For the APG case, this modification has the most significant consequences, because it alters the balance between the region where γ_f^{DP} is positive or negative, eventually leading to the change of sign observed for $\delta_e = 1.25\delta_{99}$.

The results shown here confirm, on the one hand, that a change of the upper limit of integration by an amount that is higher than 10% of δ_{99} can affect the FIK contributions significantly. As the integration limit moves farther from the wall, contributions carry progressively more information on the free-stream flow and less information on the turbulent boundary layer. In the limit $\delta_e \to \infty$, all connection between turbulence and skin friction is lost, leaving only terms related to the streamwise development of the mean velocity — as shown by Ricco and Skote (2022). On the other hand, the contributions are not significantly changed if the uncertainty in the definition of the boundary-layer thickness is of few percentage points of δ_{99}, which is compatible with focusing on the turbulent region of the domain. The sharp gradients of turbulence fluctuations generally allow to have similar or even lower uncertainties in the definition of the boundary-layer edge. Using this kind of criterion is necessary in the study of pressure-gradient turbulent boundary layers for which there is no trivial way to define U_∞ (Vinuesa et al., 2016). We thus move forward with our analysis, with the understanding that FIK contributions are sufficiently robust when the integration bound is fixed by a consistent definition of the boundary-layer edge.

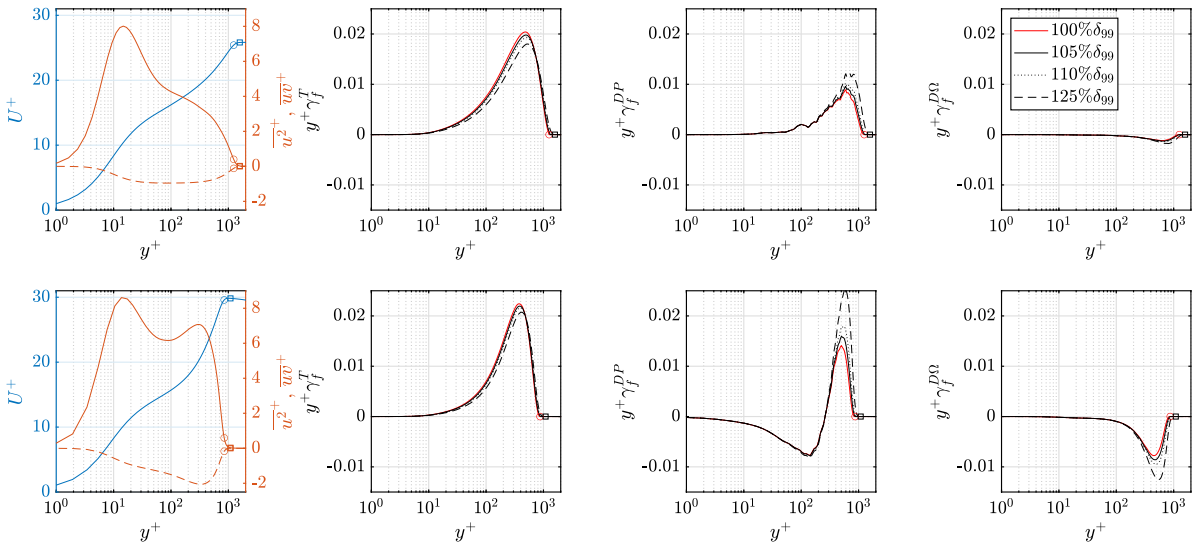

Fig. 6. Impact of the definition of the integration upper limit on the boundary-layer FIK formulation for a selected location in cases (top) ZPG and (bottom) A1.6L. In both cases, data at $Re_\theta = 4000$ are considered. (Left) Inner-scaled profiles of (blue lines) mean wall-tangential velocity, (solid red lines) $\overline{u^2}$, and (dashed red lines) $\overline{uv}$. Premultiplied profiles of the integrand of the contributions (center left) c_f^T, (center right) c_f^{DP}, and (right) $c_f^{D\Omega}$, for different definition of the boundary-layer edge. In all figures, circles and squares denote the locations of δ_{99} and $1.25\delta_{99}$, respectively. (For interpretation of the references to color in this figure legend, the reader is referred to the web version of this article.)

4.3. APG effects over the airfoil suction side

We now turn our attention to the TBL developing on the suction side of the wing profile. The TBLs on the wing profiles differ significantly from the ones analyzed so far because they eventually reach higher values of β and because β is monotonically increasing. These particular pressure-gradient conditions result in the entirety of the wing boundary layer to correspond to the portion of the flat-plate cases where β is also increasing, at least to some extent. The turbulent-fluctuation, dynamic-pressure and vorticity-convection contributions and the corresponding relative contributions for streamwise region $0.4 < x/c < 0.8$ are shown in Fig. 7, together with those of case A4.5, which is the flat-plate case that reaches the highest value of β.

The increasing value of β leads to an also increasing c_f^T contribution for all the wing cases, while the streamwise development of the dynamic-pressure and vorticity-convection contributions is more complex. Contrary to the flat-plate cases, c_f^{DP} always remains positive, although it initially decreases in the first portion of the wing profile. This is a region of relatively slow rate of change of β. In the same region, $c_f^{D\Omega}$ increases its value (*i.e.* reduces its absolute value). Further downstream however, both c_f^{DP} and $c_f^{D\Omega}$ rapidly increase in absolute values and, in case W11, eventually reach more than 10 times the value of c_f in the region considered here. The comparison between the three wing cases shows how the more intense APG in case W11 corresponds to a faster increase of the contributions than in case W5. Similarly, the lower Reynolds number in case W5(200k) also causes APG effects to be more pronounced than in case W5, although just slightly. Examining these results allows to draw a more precise comparison between the flat-plate and the wing cases. In particular, it is the second portion of the suction side that corresponds to the first portion of the flat-plate cases. The first portion of the suction side is instead more similar to region in the flat plate downstream the maximum rate of change of β. A distinction from the flat-plate cases is the fact that the streamwise evolution of $c_f^{D\Omega}$ is observed to immediately match that of c_f^{DP}. This is in contrast to what was observed before, where the evolution of c_f^{DP} anticipated that of $c_f^{D\Omega}$. Such a difference may be caused to the more abrupt evolution of the pressure condition over the airfoil suction side.

To give a more precise indication of the relative values of the contributions, we report the most-relevant terms at $x/c = 0.75$ in Table 6, together with those from case A4.5 at the location with same Re_θ of case W5 at $x/c = 0.75$. The relatively low Reynolds number causes contributions c_f^T, c_f^{DP}, and $c_f^{D\Omega}$ to account for a relatively lower portion of the total c_f with the respect to remaining terms than in the locations previously considered in Table 3. The streamwise development of c_f^δ, c^{D4}, and c_f^{D2}, however, follow the same general trend as that in case A1.6L and is not shown here. The comparison between relative contributions in cases W5 and A4.5 illustrates the difference between the two flow regimes. At the considered locations, β, Re_θ, and Re_τ have very similar values, and β is still increasing in both cases (the maximum value of β in case A4.5 is at $Re_\theta = 2600$). Nevertheless, c_f^{DP} is positive and accounts for 50% of c_f in case W5, while it is negligible in case A4.5 at this location. At the same time, the absolute value of c_f^T/c_f is higher in case A4.5 and that of $c_f^{D\Omega}/c_f$ is lower. These results constitute an additional confirmation of the relevance of history effects in APG TBLs. The comparison between cases W5 and W11 shows that the mechanism by which c_f is progressively reduced in the case of very intense APG separation is the cancellation of progressively higher contributions, where the negative term $c_f^{D\Omega}$ has the highest rate of change.

Table 6
Most-relevant skin-friction contributions for the boundary-layer formulation of the FIK identity at selected Re_θ and streamwise locations on the suction side of the airfoil and in case A4.5. The last line shows the sum of the contributions reported here, neglecting the remaining terms.

	W5(200k)	W5	W11	A4.5
x/c	0.75	0.75	0.75	–
β	3.8	3.2	20.0	3.4
Re_θ	1000	1700	2600	1700
Re_τ	220	360	320	350
c_f^T/c_f	1.81	1.66	4.79	1.97
c_f^{DP}/c_f	0.66	0.47	7.20	0.02
$c_f^{D\Omega}/c_f$	−1.66	−1.30	−11.18	−1.13
$\sum/c_f$	0.81	0.83	0.81	0.86

4.4. Flow regimes in TBL

Our observations on the skin-friction contributions for the boundary-layer FIK formulation can be summarized considering two different aspects. The first one is the sign of the dynamic-pressure

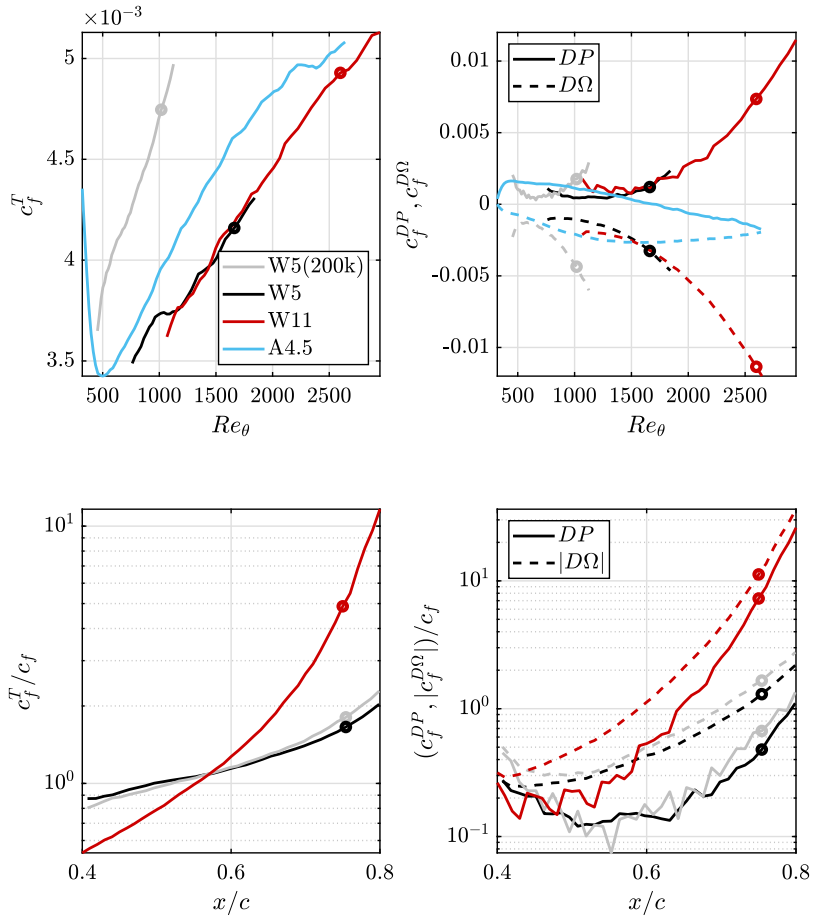

Fig. 7. (Top) Most relevant contributions for boundary-layer FIK formulation in cases W5(200k), W5, W11, and A4.5 as functions of Re_θ and (bottom) corresponding relative contributions for the wing cases as functions of x/c (note that $|c_f^{D\Omega}|$ is shown here for clarity). Only the streamwise region $0.4 < x/c < 0.8$ is shown for the wing cases and only the region up the maximum value of β for case A4.5. The circles in each plot denote location $x/c = 0.75$.

contribution, c_f^{DP}, and the second is how the rate of change of the contributions correlates with that of c_f.

Due to its definition, c_f^{DP} is zero in the case of an irrotational flow, where the total pressure P_0 is constant, following the Bernoulli equation. In the ZPG boundary layer, *i.e.* $\partial P/\partial x = 0$, the streamwise derivative of the dynamic pressure is negative and, due to the change of sign in the integration, c_f^{DP} is positive. In the APG case, $\partial P/\partial x$ is positive, and we observed that c_f^{DP} can be both positive and negative. A positive c_f^{DP} is caused by $|U(\partial U/\partial x)| > \partial P/\partial x$, *i.e.* a (negative) rate of change of the dynamic pressure in the boundary layer that is faster than that of the corresponding irrotational flow in that pressure condition. This condition implies a decrease of the total pressure. To the contrary, $c_f^{DP} < 0$ is cause by $|U(\partial U/\partial x)| < \partial P/\partial x$, *i.e.* a rate of change of the dynamic pressure that is slower than that of the corresponding irrotational flow, implying an increase of the total pressure. In the data set considered in this work, a positive dynamic-pressure contribution is connected with a rapidly increasing value of β, while a negative contribution is connected with almost uniform or decreasing β.

The rate of change of the different c_f contributions is of particular interest for possible implications in the study of separation. In principle, a reduction of c_f, eventually leading to mean separation ($c_f = 0$), could be reached either by a progressive decrease in the absolute value of all the different contributions, or by cancellation of terms with opposite sign. In the first case, the rate of the change of c_f will coincide with that of the contribution with the lowest rate of change, and the relative weight of the other contributions will remain approximately constant or decrease. This is in fact what is observed in the ZPG case, where the local c_f progressively decreases solely per effect of the Reynolds number as the boundary layer develops. In the second case (observed in APGs), contributions of different signs may have different rates of change, and the relative contributions will eventually diverge at $c_f = 0$. This is observed under certain pressure-gradient conditions; in fact, it is possible to identify three different regimes in the APG data set that we examined.

In the first regime, c_f^{DP} is positive and both c_f^T and c_f^{DP} are increasing in absolute and relative values, but $c_f^{D\Omega}$, which is negative, is decreasing at a higher rate, causing a rapid decrease of c_f. This regime is associated with a rapidly increasing value of β, and it is what we observed for case W11, where separation occurs, as well as for cases W5(200k) and W5, which have similar pressure-gradient conditions. In the second regime, c_f^{DP} is negative and c_f^{DP} and c_f^T are both decreasing, while $c_f^{D\Omega}$ is increasing (*i.e.* its absolute value decreases). This regime is observed at high Reynolds number in case A1.6L and it seems to coincide with the near-equilibrium state (Bobke et al., 2017). Despite the fact that β is still positive, the state of the boundary layer in this regime is quite similar to that of the ZPG case, in the sense that c_f has a relatively low rate of change and cancellation between terms play a minor role in determining its decrease. The third regime is an intermediate state. In this regime, β can be either increasing or decreasing, and c_f^{DP} can be either positive or negative, but it decreases. The qualitative behavior of the most relevant contributions for the various regimes are summarized in Table 7 and Fig. 8.

4.5. Control effects over the airfoil suction side

Lastly, we examine the effects of uniform blowing, body-force damping, and uniform suction on the FIK contributions for both the

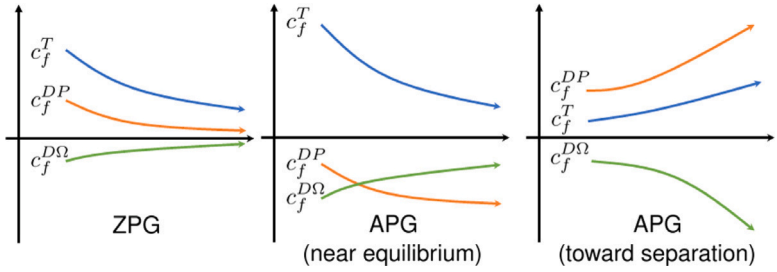

Fig. 8. Sketch of the trends of the main skin-friction contributions for the boundary-layer FIK formulation in the ZPG case and for APG near-equilibrium and towards separation (not to scale).

Table 7
Summary of the trends of the main skin-friction contributions for the boundary-layer FIK formulation in the ZPG case and in the three regimes identified in APG TBLs.

	c_f^T	c_f^{DP}	$c_f^{D\Omega}$
ZPG	Decreasing	Decreasing	Decreasing
APG: near equilibrium	Decreasing	Decreasing	Increasing
APG: towards separation	Increasing	Increasing	Decreasing
APG: intermediate	Increasing	Decreasing	(both)

standard and boundary-layer formulations, to discuss how the latter can improve the description of control applied to TBLs. We focus our attention on streamwise location $x/c = 0.75$ of the suction side of the airfoil, which is the same considered before.

The relative control effects on the standard contributions are reported in Table 8. These quantities are defined as the difference between the absolute contributions in the control and uncontrolled cases, normalized with the total c_f of the uncontrolled case. According to this definition, the sum of all relative control effects is the total relative change of c_f with respect to the uncontrolled case, which is denoted by $\Delta c_f/c_f^*$. This definition allows to identify which contribution is more relevant to describe the control effect on c_f. As already discussed (Atzori et al., 2021b), control effects on the standard FIK contributions are quite complex, which is in part a consequence of the very high absolute values of each term already in the uncontrolled case. Uniform blowing and uniform suction achieve skin-friction reduction and increase, respectively, through the wall-normal contribution c_f^{D3}. The term c_f^{D1} however is increased by an amount that is almost as high as the decrease of c_f^{D3} in uniform blowing, while the reduction of c_f^P is not negligible either (uniform suction causes similar changes in the opposite directions). In fact, the modification of the pressure-gradient contribution for both blowing and suction is higher than the total change of c_f, and even higher than the sum of the two mean-convection contributions c_f^{D1} and c_f^{D3}. This result may raise the question of whether the modification of pressure conditions above the boundary layer due to the control is in fact ultimately responsible for the change of drag, rather than a modification of momentum transfer within the boundary layer. The results for body-force damping are even more counter-intuitive. In particular, the term closely connected with the c_f reduction appears to be c_f^{D1}, which is reduced by more than twice the reduction of c_f^T. At the same time, c_f^{D3} and c_f^P are increased as a result of this control by non-negligible amounts, a fact that also does not have a clear interpretation.

The relative control effects on the contributions for the boundary-layer formulation are reported in Table 9. In the new formulation, contributions have a lower absolute values, which may also implicitly reduce relative control effects. The most significant improvement with respect to the standard formulation is a more straightforward identification of the most relevant effects. For uniform blowing and suction, the wall-normal convection contribution is still the most significantly affected. The dynamic-pressure and turbulent fluctuation contributions are increased and decreased for blowing and suction, respectively, but

Table 8
Relative effects of the control on the skin-friction contributions in the standard FIK formulation and at $x/c = 0.75$. The total skin friction of the reference case, W5, is denoted by c_f^*.

	W5BL	W5BF	W5SC
$\Delta c_f^T/c_f^*$	+0.17	−0.24	−0.21
$\Delta c_f^{D1}/c_f^*$	+1.70	**−0.55**	−1.10
$\Delta c_f^{D3}/c_f^*$	**−1.79**	+0.32	**+1.30**
$\Delta c_f^P/c_f^*$	−0.32	+0.23	+0.36
$(\Delta c_f^\delta + \Delta c_f^{D2} + \Delta c_f^{D4})/c_f^*$	−0.05	≈0	−0.03
$\Delta c_f/c_f^*$	−0.29	−0.24	+0.32

Table 9
Relative effects of the control on the skin-friction contributions in the boundary-layer FIK formulation and at $x/c = 0.75$. The total skin friction of the reference case, W5, is denoted by c_f^*.

	W5BL	W5BF	W5SC
$\Delta c_f^T/c_f^*$	+0.17	**−0.24**	−0.21
$\Delta c_f^{DP}/c_f^*$	+0.55	−0.05	−0.19
$\Delta c_f^{D\Omega}/c_f^*$	**−0.96**	+0.05	**+0.75**
$(\Delta c_f^\delta + \Delta c_f^{D2} + \Delta c_f^{D4})/c_f^*$	−0.05	≈0	−0.03
$\Delta c_f/c_f^*$	−0.29	−0.24	+0.32

by a relatively lower amount. These results show that the modification of vorticity convection is indeed the main mechanism affecting friction for wall-transpiration. In the case of body-force damping, the modification of the dynamic-pressure and vorticity convection are now significantly lower than that of c_f^T, showing that the reduction of turbulent fluctuations is indeed the prevalent control effect in this case.

5. Conclusions

This paper is dedicated to stress the significance of a physically meaningful aggregation of skin-friction contributions in the study of adverse-pressure-gradient turbulent boundary layers. We encounter many challenges in the application of skin-friction decompositions such as the FIK identity in the case of APG TBLs. For instance, the definition of the upper bound of integration has received significant attention in the literature. Yet, the skin-friction contributions remain similar if the integration bound varies within the uncertainty of a robust definition for the boundary-layer edge. Contributions will naturally change more significantly when they are computed in different portions of the domain, *e.g.* multiple δ_{99} lengths instead of one. This issue however is as much related to the contributions as to the definition of a region of interest.

We compared the contributions of the FIK decomposition derived with the original procedure with a new formulation specifically designed for boundary layers In this formulation, pressure gradient and wall-tangential convection are considered together in a dynamic-pressure contribution.

We examined the results of both FIK formulations in a number of cases and found that the new contribution allows a more effective description of pressure-gradient effects. In cases with moderate pressure gradient the dynamic-pressure contribution represents the balance between mean-convection and pressure-gradient terms in the averaged governing equations, highlighting the role of turbulent fluctuations. The new contribution also enables distinguishing between different states of turbulent boundary layers subjected to an intense pressure gradient, changing sign in the transition between rapidly increasing and constant or decreasing values of the Clauser parameter. It is then possible to establish a criterion to define the regimes of near-equilibrium condition and that of approaching separation. The dynamic-pressure contribution also improves the description of control effects. In cases with uniform blowing and suction, skin-friction reduction or increase are directly related to an increase or reduction, respectively, of the wall-normal convection of vorticity. In the case of body-force damping, control effects are limited to the turbulent-fluctuation contributions.

Finally, while we focused on the FIK identity derived using the original triple integration by parts, the idea of considering streamwise development of the dynamic pressure and static pressure together can be applied to any decomposition that is also derived from integration of the averaged governing equations. In the RD decomposition, for example, we observe similar cancellations between contributions as in the FIK decomposition, when the corresponding terms or groups of terms are compared.

There are a number of important points that we did not investigate and leave to future studies. Firstly, regardless of its impact on general results, the crucial question of whether it actually makes sense to impose a quantity such as δ_{99} as upper integration bound remains open. We used the FIK decomposition in this paper with the idea of analyzing contributions within the boundary layer, but the mean location of the edge remains a somehow artificial choice. One possibility for further development in this direction may be to use *e.g.* an intermittency-based criterion to restrict the analysis on statistics sampled for the turbulent flow only. Similar strategies has been already considered for mean profiles (Kwon et al., 2016) and coherent structures (Hwang and Sung, 2018; Atzori et al., 2020). A second point is how to properly quantify the development of the adverse pressure gradient, which our results strongly suggest to be the defining factor for different flow regimes. We relied solely on the Clauser parameter and our analysis remained qualitative under this perspective. Lastly, there is the question of whether skin-friction decompositions can aid in the study of the onset of mean separation, which is related to both previous points. Even though we considered one case where mean separation occurs, we focused on a domain region well upstream of the separation point. This is because the edge identification and the characterization of pressure-gradient conditions become even more challenging in the proximity of separation. Addressing these points in a more systematic way is the prerequisite to further investigate the connection between the evolution of skin-friction contributions and the occurrence of mean separation.

CRediT authorship contribution statement

Marco Atzori: Writing – original draft, Software, Formal analysis, Data curation, Conceptualization. **Fermín Mallor:** Writing – review & editing, Software, Data curation, Visualization. **Ramón Pozuelo:** Software, Data curation. **Koji Fukagata:** Writing – review & editing, Formal analysis, Conceptualization. **Ricardo Vinuesa:** Writing – review & editing, Conceptualization, Project administration, Funding acquisition, Supervision. **Philipp Schlatter:** Writing – review & editing, Resources, Conceptualization, Project administration, Funding acquisition, Supervision.

Declaration of competing interest

The authors declare that they have no known competing financial interests or personal relationships that could have appeared to influence the work reported in this paper.

Data availability

Data will be made available on request.

Acknowledgments

We thank Perry L. Johnson (University of California, Irvine) for discussions on how to extend the angular momentum integral to adverse-pressure-gradient turbulent boundary layers. M.A. acknowledges financial support of the Austrian Science Fund (FWF), project number: I5180-N. R.P and R.V. acknowledge financial support provided by the Swedish Research Council (VR). F.M. and P.S. acknowledge financial support provided by the Knut and Alice Wallenberg Foundation, Sweden. K.F. acknowledges the financial support provided by Japan Society for Promotion of Science (JSPS), grant number: 21H05007. Part of the computations and data handling were enabled by resources provided by the Swedish National Infrastructure for Computing (SNIC), partially funded by the Swedish Research Council through grant agreement no. 2018-05973. Parts of the computations were also performed on the EuroHPC system LUMI using grant number EHPC-REG-2021R0088.

Appendix A. Dynamic-pressure contribution in the RD decomposition

The RD decomposition is derived with the aim of connecting turbulent-kinetic-energy budget and generation of skin-friction (Renard and Deck, 2016). With respect to the FIK decomposition, the resulting integrands of each contribution have more intuitive scaling properties. Nevertheless, in the APG case the total c_f is still recovered as a results of cancellation between different terms with high absolute values (Fan et al., 2020b; Atzori et al., 2021b). We denote the RD contributions as follow:

$$c_f = c_f^{Pr} + c_f^{\varepsilon} + (c_f^{CU} + c_f^{CV}) + c_f^{Diff} + c_f^{P(RD)}. \tag{A.1}$$

The first two contributions are related to turbulent production and dissipation, respectively, and the last term is the work exerted by the pressure gradient. The remaining terms are due to energy transport and are usually separated between diffusion, denoted by c_f^{Diff}, and mean convection. In the present case, we distinguish between convection due to the streamwise and wall-normal mean velocity, denoted by c_f^{CU} and c_f^{CV}, respectively. The definition of each term is reported below:

$$c_f^{Pr} = \frac{2}{U_e^3}\int_0^{\delta_{99}} -\overline{uv}\frac{\partial U}{\partial y}\,\mathrm{d}y, \tag{A.2}$$

$$c_f^{\varepsilon} = \frac{2}{U_e^3}\int_0^{\delta_{99}} \nu\left(\frac{\partial U}{\partial y}\right)^2\mathrm{d}y, \tag{A.3}$$

$$c_f^{CU} = \frac{2}{U_e^3}\int_0^{\delta_{99}} (U-U_e)\left(U\frac{\partial U}{\partial x}\right)\mathrm{d}y, \tag{A.4}$$

$$c_f^{CV} = \frac{2}{U_e^3}\int_0^{\delta_{99}} (U-U_e)\left(V\frac{\partial U}{\partial y}\right)\mathrm{d}y, \tag{A.5}$$

$$c_f^{Diff} = \frac{2}{U_e^3}\int_0^{\delta_{99}} -(U-U_e)\left(\nu\frac{\partial^2 U}{\partial x^2} - \frac{\partial \overline{u^2}}{\partial x}\right)\mathrm{d}y, \tag{A.6}$$

$$c_f^{P(RD)} = \frac{2}{U_e^3}\int_0^{\delta_{99}} (U-U_e)\left(\frac{1}{\rho}\frac{\partial P}{\partial x}\right)\mathrm{d}y. \tag{A.7}$$

In this form, the RD contributions can be compared with the FIK contributions derived from the convective form of the Navier–Stokes equation, *e.g.* c_f^{CU} corresponds to c_f^{D1*}. We can also introduce a term associated with the vorticity, $c_f^{C\Omega}$, and the dynamic-pressure contribution, $c_f^{DP(RD)}$, following the same procedure for the boundary-layer formulation of the FIK identity. The values of the FIK and RD contributions in both formulations are reported in Table A.10 for two location in case A1.6L.

Table A.10
Relative contributions for the FIK and RD decompositions and both standard and boundary-layer formulations at two location in case A1.6L.

FIK			RD		
β	1.2	1.4	β	1.2	1.4
Re_θ	2000	6000	Re_θ	2000	6000
Re_τ	530	1200	Re_τ	530	1200
c_f^T/c_f	1.20	1.70	c_f^{Pr}/c_f	0.81	1.10
c_f^δ/c_f	0.07	0.04	c_f^ϵ/c_f	0.35	0.30
c_f^{D1*}/c_f	1.80	1.60	c_f^{CU}/c_f	1.30	1.30
c_f^{D3*}/c_f	−0.37	−0.30	c_f^{CV}/c_f	−0.29	−0.26
c_f^P/c_f	−1.70	−2.00	$c_f^{P(RD)}/c_f$	−1.20	−1.50
c_f^{DP}/c_f	0.08	−0.42	$c_f^{DP(RD)}/c_f$	0.14	−0.12
$c_f^{D\Omega}/c_f$	−0.38	−0.30	$c_f^{C\Omega}/c_f$	−0.29	−0.26
$\sum_X c_f^X/c_f$	0.99	1.00	$\sum_X c_f^X/c_f$	1.00	1.00

As already discussed for case W5 by Atzori et al. (2021b), the values of RD and FIK contributions are relatively similar. In particular, for both identities the APG results in very high values of the positive wall-tangential convection and the negative pressure-gradient contributions. As for the FIK decomposition, these contributions are higher than the turbulent fluctuations one. On the other hand, in the novel boundary-layer formulation, $c_f^{DP(RD)}/c_f$ is lower than both c_f^{Pr}/c_f and c_f^ϵ/c_f, and it also exhibits a similar change of sign as for the corresponding term in the FIK decomposition. Modification of control effects are also similar to those in the boundary-layer FIK formulation (not shown here).

Appendix B. Dynamic-pressure contribution and AMI

The angular-momentum-integral (AMI) decomposition (Elnahhas and Johnson, 2022) has been proposed to describe the generation of skin friction in TBLs in terms of discrepancy with respect to the laminar solution. With this goal, the decomposition is derived in terms of the defect profiles from the von Kármán momentum integral, starting from the following expression:

$$\frac{\partial(U_\infty - U)U}{\partial x} + \frac{\partial(U_\infty - U)V}{\partial y} + (U_\infty - U)\frac{\partial U_\infty}{\partial x} = \\ = -\nu\frac{\partial^2 U}{\partial y^2} + \frac{\partial \overline{uv}}{\partial y} - I_x\,, \tag{B.1}$$

where the term I_x, for the stationary case, is written as:

$$I_x = +\frac{1}{\rho}\frac{\partial(P_\infty - P)}{\partial x} + \nu\frac{\partial^2 U}{\partial x^2} - \frac{\partial \overline{u^2}}{\partial x}\,. \tag{B.2}$$

The skin-friction decomposition is then derived in terms of generalized momentum thickness and displacement thickness, introducing a characteristic length scale l, which needs to be specified:

$$\frac{1}{2}c_f = \frac{1}{Re_l} + \int_0^\infty -\frac{\overline{uv}}{U_\infty^2 l}\mathrm{d}y + \frac{\partial\theta_l}{\partial x} - \frac{\theta-\theta_l}{l}\frac{\mathrm{d}l}{\mathrm{d}x} + \\ + \frac{\theta_v}{l} + \frac{\delta_l^* + 2\theta_l}{U_\infty}\frac{\partial U_\infty}{\partial x} + I_{x,l}\,, \tag{B.3}$$

where $Re_l = U_\infty l/\nu$ and $I_{x,l}$, δ_l^*, θ_l, and θ_v denote:

$$I_{x,l} = \int_0^\infty \left(1-\frac{y}{l}\right)\frac{I_x}{U_\infty}\mathrm{d}y\,, \\ \delta_l^* = \int_0^\infty \left(1-\frac{y}{l}\right)\left(1-\frac{U(y)}{U_\infty}\right)\mathrm{d}y\,, \\ \theta_l = \int_0^\infty \left(1-\frac{y}{l}\right)\left(1-\frac{U(y)}{U_\infty}\right)\frac{U(y)}{U_\infty}\mathrm{d}y\,, \\ \theta_v = \int_0^\infty \left(1-\frac{U(y)}{U_\infty}\right)\frac{V(y)}{U_\infty}\mathrm{d}y\,. \tag{B.4}$$

In this decomposition, the defect streamwise development and pressure-gradient terms are still present, and could be used to formally define a dynamic-pressure contributions *e.g.* combining pressure gradient and streamwise derivative of the defect profile $U_\infty - U$ in expressions (B.1) and (B.2). The AMI, as currently formulated, is well-suited for ZPG TBL and should also be effective for analyzing weak APGs ($\beta \approx 1$). Expression (B.1) however is not the most suitable to create a skin-friction decomposition for TBL subjected to strong APG, for which the boundary-layer approximation and thus the von Kármán integral are not necessarily verified. The more natural generalization of the AMI is instead to define defect profiles based on a more general expression that does not rely on the boundary-layer approximation. From that form, it could then be determined whether a dynamic-pressure contribution can be defined, to further distinguish between different contributions.

References

Alfredsson, P.H., Segalini, A., Örlü, R., 2011. A new scaling for the streamwise turbulence intensity in wall-bounded turbulent flows and what it tells us about the 'outer' peak. Phys. Fluids 23, 041702.

Atzori, M., Vinuesa, R., Lozano-Durán, A., Schlatter, P., 2020. Coherent structures in turbulent boundary layers over an airfoil. J. Phys. Conf. Ser. 1522 (1), 012020. http://dx.doi.org/10.1088/1742-6596/1522/1/012020.

Atzori, M., Vinuesa, R., Lozano-Durán, A., Schlatter, P., 2021a. Intense Reynolds-stress events in turbulent ducts. Int. J. Heat Fluid Flow 89, 108802.

Atzori, M., Vinuesa, R., Stroh, A., Gatti, D., Frohnapfel, B., Schlatter, P., 2021b. Uniform blowing and suction applied to non-uniform adverse-pressure-gradient wing boundary layers. Phys. Rev. Fluids 6, 113904.

Bobke, A., Örlü, R., Schlatter, P., 2016. Simulations of turbulent asymptotic suction boundary layers. J. Turbul. 17 (2), 157–180.

Bobke, A., Vinuesa, R., Örlü, R., Schlatter, P., 2017. History effects and near-equilibrium in adverse-pressure-gradient turbulent boundary layers. J. Fluid Mech. 820, 667–692.

Chauhan, K., Philip, J., de Silva, C.M., Hutchins, N., Marusic, I., 2014. The turbulent/non-turbulent interface and entrainment in a boundary layer. J. Fluid Mech. 742, 119–151.

Chevalier, M., Schlatter, P., Lundbladh, A., Henningson, D., 2007. A Pseudo-Spectral Solver for Incompressible Boundary Layer Flow. Tech. Rep. TRITA-MEK 2007:07, Royal Institute of Technology, Stockholm, Sweden.

Clauser, F., 1956. The turbulent boundary layer. Adv. Appl. Mech. 4, 1–51.

Dong, S., Karniadakis, G.E., Chryssostomidis, C., 2014. A robust and accurate outflow boundary condition for incompressible flow simulations on severely-truncated unbounded domains. J. Comput. Phys. 261, 83–105.

Drózdz, A., Elsner, W., Drobniak, S., 2015. Scaling of streamwise Reynolds stress for turbulent boundary layers with pressure gradient. Eur. J. Mech. B-Fluids 49, 137–145.

Eitel-Amor, G., Örlü, R., Schlatter, P., 2014. Simulation and validation of a spatially evolving turbulent boundary layer up to $Re_\theta = 8300$. Int. J. Heat Fluid Flow 47, 57–69.

Elnahhas, A., Johnson, P.L., 2022. On the enhancement of boundary layer skin friction by turbulence: an angular momentum approach. J. Fluid Mech. 940, A36. http://dx.doi.org/10.1017/jfm.2022.264.

Fan, Y., Atzori, M., Vinuesa, R., Gatti, D., Schlatter, P., Li, W., 2022. Decomposition of the mean friction drag on an NACA4412 airfoil under uniform blowing/suction. J. Fluid Mech. 932, A31. http://dx.doi.org/10.1017/jfm.2021.1015.

Fan, Y.-T., Li, W.-P., Atzori, M., Pozuelo, R., Schlatter, P., Vinuesa, R., 2020a. Decomposition of the mean friction drag in adverse-pressure-gradient turbulent boundary layers. Phys. Rev. Fluids 5, 114608.

Fan, Y., Li, W., Atzori, M., Pozuelo, R., Schlatter, P., Vinuesa, R., 2020b. Decomposition of the mean friction drag in adverse-pressure-gradient turbulent boundary layers. Phys. Rev. Fluids 5, 114608. http://dx.doi.org/10.1103/PhysRevFluids.5.114608, URL: https://link.aps.org/doi/10.1103/PhysRevFluids.5.114608.

Fan, Y.-T., Li, W.-P., Pirozzoli, S., 2020c. Energy-based decomposition of friction drag in turbulent square-duct flows. Int. J. Heat Fluid Flow (ISSN: 0142-727X) 86, 108731.

Fischer, P., Kruse, J., Mullen, J., Tufo, H., Lottes, J., Kerkemeier, S., 2008. Nek5000: open source spectral element CFD solver. Available at http://nek5000.mcs.anl.gov/.

Fukagata, K., Iwamoto, K., Kasagi, N., 2002. Contribution of Reynolds stress distribution to the skin friction in wall-bounded flows. Phys. Fluids 14 (11), L73–L76.

Griffin, K.P., Fu, L., Moin, P., 2021. General method for determining the boundary layer thickness in nonequilibrium flows. Phys. Rev. Fluids 6, 024608. http://dx.doi.org/10.1103/PhysRevFluids.6.024608, URL: https://link.aps.org/doi/10.1103/PhysRevFluids.6.024608.

Hosseini, S.M., Vinuesa, R., Schlatter, P., Hanifi, A., Henningson, D.S., 2016. Direct numerical simulation of the flow around a wing section at moderate Reynolds number. Int. J. Heat Fluid Flow 61, 117–128.

Hwang, J., Sung, H., 2018. Wall-attached structures of velocity fluctuations in a turbulent boundary layer. J. Fluid Mech. 856, 958–983.

Jeong, J., Hussain, F., 1995. On the identification of a vortex. J. Fluid Mech. 285, 69–94.

Kametani, Y., Fukagata, K., 2011. Direct numerical simulation of spatially developing turbulent boundary layers with uniform blowing or suction. J. Fluid Mech. 681, 154–172.

Kametani, Y., Fukagata, K., Örlü, R., Schlatter, P., 2015. Effect of uniform blowing/suction in a turbulent boundary layer at moderate Reynolds number. Int. J. Heat Fluid Flow 55, 134–142.

Kwon, Y., Hutchins, N., Monty, J., 2016. On the use of the Reynolds decomposition in the intermitten region of turbulent boundary layers. J. Fluid Mech. 794, 5–16.

Li, W.-P., Fan, Y.-T., Modesti, D., Cheng, C., 2019. Decomposition of the mean skin-friction drag in compressible turbulent channel flows. J. Fluid Mech. 875, 101–123.

Mavriplis, C., 1990. A posteriori error estimators for adaptive spectral element techniques. In: Wesseling, P. (Ed.), Notes on Numerical Fluid Mechanics. pp. 333–342.

Mehdi, F., Johansson, T.G., White, C.M., Naughton, J.W., 2014. On determining wall shear stress in spatially developing two-dimensional wall-bounded flows. Exp. Fluids 55 (1), 1656.

Mehdi, F., White, C.M., 2011. Integral form of the skin friction coefficient suitable for experimental data. Exp. Fluids 50 (1), 43–51.

Modesti, D., Pirozzoli, S., Orlandi, P., Grasso, F., 2018. Turbulence and secondary motions in square duct flow. J. Fluid Mech. 847, R1.

Monte, S., Sagaut, P., Gomez, T., 2011. Analysis of turbulent skin friction generated in flow along a cylinder. Phys. Fluids 23 (6), 065106. http://dx.doi.org/10.1063/1.3590018.

Negi, P., Vinuesa, R., Hanifi, A., Schlatter, P., Henningson, D., 2018. Unsteady aerodynamic effects in small-amplitude pitch oscillations of an airfoil. Int. J. Heat Fluid Flow 72, 378–391.

Patera, A.T., 1984. A spectral element method for fluid dynamics: laminar flow in a channel expansion. J. Comput. Phys. 54, 468–488.

Peet, Y., Sagaut, P., 2009. Theoretical prediction of turbulent skin friction on geometrically complex surfaces. Phys. Fluids 21 (10), 105105.

Pozuelo, R., Li, Q., Schlatter, P., Vinuesa, R., 2022. An adverse-pressure-gradient turbulent boundary layer with nearly constant $\beta \simeq 1.4$ up to $Re_\theta \simeq 8700$. J. Fluid Mech. 939, A34.

Renard, N., Deck, S., 2016. A theoretical decomposition of mean skin friction generation into physical phenomena across the boundary layer. J. Fluid Mech. 790, 339–367. http://dx.doi.org/10.1017/jfm.2016.12.

Ricco, P., Skote, M., 2022. Integral relations for the skin-friction coefficient of canonical flows. J. Fluid Mech. 943, A50. http://dx.doi.org/10.1017/jfm.2022.444.

Schlatter, P., Örlü, R., 2010. Assessment of direct numerical simulation data of turbulent boundary layers. J. Fluid Mech. 659, 116–126.

Schlatter, P., Örlü, R., 2012. Turbulent boundary layers at moderate Reynolds numbers: inflow length and tripping effects. J. Fluid Mech. 710, 5–34.

Schlatter, P., Stolz, S., Kleiser, L., 2004. LES of transitional flows using the approximate deconvolution model. Int. J. Heat Fluid Flow 25, 549–558.

Stroh, A., Frohnapfel, B., Schlatter, P., Hasegawa, Y., 2015. A comparison of opposition control in turbulent boundary layer and turbulent channel flow. Phys. Fluids 27, 075101.

Stroh, A., Hasegawa, Y., Schlatter, P., Frohnapfel, B., 2016. Global effect of local skin friction drag reduction in spatially developing turbulent boundary layer. J. Fluid Mech. 805, 303–321.

Tanarro, A., Mallor, F., Offermans, N., Peplinski, A., Vinuesa, R., Schlatter, P., 2020. Enabling adaptive mesh refinement for spectral-element simulations of turbulence around wing sections. Flow Turbul. Combust. 105, 415–436. http://dx.doi.org/10.1007/s10494-020-00152-y.

Vila, C.S., Vinuesa, R., Discetti, S., Ianiro, A., Schlatter, P., Örlü, R., 2020. Experimental realisation of near-equilibrium adverse-pressure-gradient turbulent boundary layers. Exp. Therm. Fluid Sci. 112, 109975. http://dx.doi.org/10.1016/j.expthermflusci.2019.109975, URL: http://www.sciencedirect.com/science/article/pii/S0894177719309896.

Vinuesa, R., Bobke, A., Örlü, R., Schlatter, P., 2016. On determining characteristic length scales in pressure-gradient turbulent boundary layers. Phys. Fluids 28, 055101.

Vinuesa, R., Negi, P., Atzori, M., Hanifi, A., Henningson, D., Schlatter, P., 2018. Turbulent boundary layers around wing sections up to $Re_c = 1,000,000$.. Int. J. Heat Fluid Flow 72, 86–99.

Wei, T., 2018. Integral properties of turbulent-kinetic-energy production and dissipation in turbulent wall-bounded flows. J. Fluid Mech. 854, 449–473.

Wenzel, C., Gibis, T., Kloker, M., 2022. About the influences of compressibility, heat transfer and pressure gradients in compressible turbulent boundary layers. J. Fluid Mech. 930, A1. http://dx.doi.org/10.1017/jfm.2021.888.

Yoon, M., Ahn, J., Hwang, J., Sung, H.J., 2016. Contribution of velocity-vorticity correlations to the frictional drag in wall-bounded turbulent flows. Phys. Fluids 28 (8), 081702.